Ion-ion model collision operators: a Krook operator and a model Fokker-Planck operator

M. R. Hardman[1,2], J. Omotani[3], M. Barnes[2], S. L. Newton[3], and F. I. Parra[4]

[1] Tokamak Energy Ltd, 173 Brook Drive, Milton Park, Abingdon, OX14 4SD, United Kingdom

[2] Rudolf Peierls Centre for Theoretical Physics, University of Oxford, Clarendon Laboratory, Parks Road, Oxford OX1 3PU, United Kingdom

[3] United Kingdom Atomic Energy Authority, Culham Science Centre, Abingdon, Oxon, OX14 3DB, UK

[4] Princeton Plasma Physics Laboratory, P.O. Box 451, Princeton, New Jersey 08540, United States

E-mail: michael.hardman@tokamakenergy.co.uk

1. Introduction

In this report, we explore model collision operators for ion-ion collisions. Ion-ion collisions are crucial for accurate descriptions of the plasma for several reasons. Firstly, in the hot core of the plasma, ion-ion collisions drive the ion distribution function towards a Maxwellian distribution that is parameterised by a density, mean velocity, and temperature [1, 2]. Considering the small turbulent fluctuations that perturb the dominant Maxwellian distribution, the ion-ion collisions regularise the complicated kinetic ion distribution function by dissipating fine structures in velocity space [3, 4]. In the edge, the plasma transitions from the hot core-like conditions to a much colder plasma near the divertor target. Because of the change in temperature, the Fokker-Planck collision frequency becomes larger, potentially forcing the ion distribution function closer to a Maxwellian and making even the turbulent fluctuations close to a Maxwellian response. However, at the divertor target itself the absorbing ion boundary condition implies that a Maxwellian distribution is not the solution for the ion distribution function – to find the form of the ion distribution near the divertor target we need to include an accurate collision operator and discover how the operator interacts with the wall boundary conditions [5].

Recent PhD work by M Abazorius explores a simplified 1D2V model of ions in the collisional pre-sheath with the exact Fokker-Planck ion collision operator [6] and Boltzmann electrons [5] – this work shares common features with our model development, such as finite-element methods. However, the work in [5] solves only steady-state problems, requiring a new model implementation for the time-evolving problem.

In this report, we consider a 1D2V model of a simple two species plasma consisting of a drift kinetic model of ions and Boltzmann electrons. For the collision operator we consider a model Krook operator [7]. We test our implementation of the Krook operator using manufactured solutions tests. We also document the initial stages of our work in progress implementing the full Fokker-Planck operator. We begin by implementing a model Fokker-Planck operator and we develop analytical functional tests. Whilst we have not yet implemented the full, exact Fokker-Planck operator, our results may influence future development.

2. The 1D2V model of the plasma

The ion distribution function F_i is evolved with the drift-kinetic equation [8]:

$$\frac{\partial F_i}{\partial t} + b_z v_\parallel \frac{\partial F_i}{\partial z} + \frac{e b_z E_z}{m_i}\frac{\partial F_i}{\partial v_\parallel} = C_{ii}\left[F_i, F_i^M\right] + \nu_K\left(F_i^M - F_i\right) + \nu_\parallel \frac{\partial^2 F_i}{\partial {v_\parallel}^2} + S_i, \tag{1}$$

where $v_\parallel = \mathbf{v}\cdot\mathbf{b}$ and $v_\perp = |\mathbf{v} - v_\parallel \mathbf{b}|$ are the components of the particle velocity $\mathbf{v}$ that are parallel and perpendicular to the magnetic field direction $\mathbf{b} = \mathbf{B}/B$, respectively, with B the magnetic field strength. The frequency ν_K is an effective, constant, collision frequency, F_i^M is a Maxwellian distribution formed from the first three velocity moments of F_i, i.e.,

$$F_i^M = \frac{n_i}{\pi^{3/2} v_{\mathrm{th,i}}^3}\exp\left[-\frac{(v_\parallel - u_{\parallel i})^2 + v_\perp^2}{v_{\mathrm{th,i}}^2}\right], \tag{2}$$

and the collision operator $C_{ii}\left[F_i, F_i^M\right]$ is the modified Fokker-Planck operator, which we describe in the next section. The variable t is the time, $b_z = B_z/B$, ϕ is the electrostatic potential, $\nu_\parallel$ is a numerical diffusion coefficient, and S_i is a source function that may be used to inject particles, momentum, and heat, or to facilitate a test via the method of manufactured solutions.

The electrostatic potential is computed by enforcing quasineutrality $n_i = n_e$ and using a Boltzmann response for electrons, i.e.,

$$n_i = n_e = N_e \exp\left(\frac{e\phi}{T_e}\right), \tag{3}$$

where the constant N_e is either taken to be a reference density, or calculated through a simple electron sheath model. The ion density n_i is computed by integrating over the ion distribution function:

$$n_i(z, r, t) = 2\pi \int_{-\infty}^{\infty} dv_\parallel \int_0^\infty dv_\perp v_\perp F_i(z, r, v_\perp, v_\parallel, t). \tag{4}$$

We obtain the electric fields by differentiation of ϕ:

$$E_z = -\frac{\partial \phi}{\partial z}, \text{ and } \quad E_r = -\frac{\partial \phi}{\partial r}. \tag{5}$$

3. The Fokker-Planck collision operator

The full Fokker-Planck operator for collisions between species indexed by s and s' with distribution functions $F_s = F_s(\mathbf{v})$ and $F_{s'} = F_{s'}(\mathbf{v})$, respectively, is [6, 9]

$$C_{ss'}\left[F_s, F_{s'}\right] = \frac{\gamma_{ss'}}{m_s}\frac{\partial}{\partial \mathbf{v}} \cdot \left\{ \int \frac{\partial^2 g}{\partial \mathbf{v} \partial \mathbf{v}} \cdot \left[\frac{F_{s'}(\mathbf{v}')}{m_s}\frac{\partial F_s}{\partial \mathbf{v}} - \frac{F_s(\mathbf{v})}{m_{s'}}\frac{\partial F_{s'}}{\partial \mathbf{v}'} \right] d^3\mathbf{v}' \right\}, \tag{6}$$

where

$$\gamma_{ss'} = \frac{2\pi Z_s^2 {Z_{s'}}^2 e^4 \ln \Lambda_{ss'}}{(4\pi\epsilon_0)^2} \tag{7}$$

and

$$g = |\mathbf{v} - \mathbf{v}'|. \tag{8}$$

It is useful to reduce the collision operator to the drift-kinetic case where the distribution functions are independent of gyroangle, i.e., $F_s = F_s(v_\parallel, v_\perp)$ and $F_{s'} = F_{s'}(v_\parallel, v_\perp)$. We write the operator in the Rosenbluth-MacDonald-Judd (RMJ) form

$$C_{ss'}\left[F_s, F_{s'}\right] = \frac{\partial \Gamma_\parallel}{\partial v_\parallel} + \frac{1}{v_\perp}\frac{\partial}{\partial v_\perp}\left(v_\perp \Gamma_\perp\right). \tag{9}$$

with the fluxes

$$\Gamma_\parallel = \frac{\gamma_{ss'}}{m_s^2}\left(\frac{\partial F_s}{\partial v_\parallel}\frac{\partial^2 G_{s'}}{\partial {v_\parallel}^2} + \frac{\partial F_s}{\partial v_\perp}\frac{\partial^2 G_{s'}}{\partial v_\perp \partial v_\parallel} - 2\frac{m_s}{m_{s'}}F_s\frac{\partial H_{s'}}{\partial v_\parallel} \right), \tag{10}$$

and

$$\Gamma_\perp = \frac{\gamma_{ss'}}{m_s^2}\left(\frac{\partial F_s}{\partial v_\parallel}\frac{\partial^2 G_{s'}}{\partial v_\parallel \partial v_\perp} + \frac{\partial F_s}{\partial v_\perp}\frac{\partial^2 G_{s'}}{\partial {v_\perp}^2} - 2\frac{m_s}{m_{s'}}F_s\frac{\partial H_{s'}}{\partial v_\perp} \right), \tag{11}$$

where the Rosenbluth potentials are

$$G_{s'}(\mathbf{v}) = \int F_{s'}(\mathbf{v}')g \; d^3\mathbf{v}' \tag{12}$$

and

$$H_{s'}(\mathbf{v}) = \int \frac{F_{s'}(\mathbf{v}')}{g} \; d^3\mathbf{v}'. \tag{13}$$

In terms of $(v_\parallel, v_\perp)$ coordinates, the Rosebluth potentials simplify to

$$G_{s'} = \int_0^\infty \int_{-\infty}^\infty 4\left(\left(v_\parallel - v'_\parallel\right)^2 + \left(v_\perp + v'_\perp\right)^2 \right)^{1/2} E(k(v_\parallel, v_\perp, v'_\parallel, v'_\perp)) F_{s'}(v'_\parallel, v'_\perp) v'_\perp \; dv'_\parallel dv'_\perp, \tag{14}$$

and

$$H_{s'} = \int_0^\infty \int_{-\infty}^\infty 4\left(\left(v_\parallel - v'_\parallel\right)^2 + \left(v_\perp + v'_\perp\right)^2 \right)^{-1/2} K(k(v_\parallel, v_\perp, v'_\parallel, v'_\perp)) F_{s'}(v'_\parallel, v'_\perp) v'_\perp \; dv'_\parallel dv'_\perp, \tag{15}$$

where

$$k(v_\parallel, v_\perp, v'_\parallel, v'_\perp) = 2(v_\perp v'_\perp)^{1/2}\left(\left(v_\parallel - v'_\parallel\right)^2 + \left(v_\perp + v'_\perp\right)^2 \right)^{-1/2}, \tag{16}$$

and we have used the definitions of the complete elliptic integral of the first kind

$$K(k) = \int_0^{\pi/2} \frac{1}{\sqrt{1 - k^2 \sin^2\theta}}\, d\theta \tag{17}$$

and the complete elliptic integral of the second kind

$$E(k) = \int_0^{\pi/2} \sqrt{1 - k^2 \sin^2\theta}\, d\theta. \tag{18}$$

3.1. Rosenbluth potentials for shifted Maxwellian distributions

It is useful to compute these potentials for the shifted Maxwellian distribution

$$F_{s'}^M(\mathbf{v}) = \frac{n_{s'}}{\pi^{3/2} v_{\mathrm{th},s'}^3} \exp\left[-\frac{(\mathbf{v} - \mathbf{u}_{s'})^2}{v_{\mathrm{th},s'}^2}\right]. \tag{19}$$

The results for a Maxwellian distribution centred on $\mathbf{u}_{s'} = 0$ are given by [9]

$$G_{s'}(\mathbf{v}) = n_{s'} v_{\mathrm{th},s'} \mathcal{G}(\eta) = \frac{n_{s'} v_{\mathrm{th},s'}}{2\eta} \left(\frac{2\eta}{\sqrt{\pi}} \exp\left[-\eta^2\right] + (1 + 2\eta^2)\,\mathrm{erf}(\eta)\right), \tag{20}$$

and

$$H_{s'}(\mathbf{v}) = \frac{n_{s'}}{v_{\mathrm{th},s'}} \mathcal{H}(\eta) = \frac{n_{s'}}{v_{\mathrm{th},s'}} \frac{\mathrm{erf}(\eta)}{\eta}, \tag{21}$$

with $\eta = |\mathbf{v}|/v_{\mathrm{th},s'}$. For the case where $\mathbf{u}_{s'} \neq 0$ we can find a very similar result

$$\begin{aligned} G_{s'}(\mathbf{v}) &= \int \frac{n_{s'}}{\pi^{3/2} v_{\mathrm{th},s'}^3} \exp\left[-\frac{(\mathbf{v} - \mathbf{u}_{s'})^2}{v_{\mathrm{th},s'}^2}\right] |\mathbf{v} - \mathbf{v}'|\, d^3\mathbf{v}' \\ &= \int \frac{n_{s'}}{\pi^{3/2} v_{\mathrm{th},s'}^3} \exp\left[-\frac{|\mathbf{w}'|^2}{v_{\mathrm{th},s'}^2}\right] |(\mathbf{v} - \mathbf{u}_{s'}) - \mathbf{w}'|\, d^3\mathbf{w}' \\ &= n_{s'} v_{\mathrm{th},s'} \mathcal{G}\left(\frac{|\mathbf{v} - \mathbf{u}_{s'}|}{v_{\mathrm{th},s'}}\right), \end{aligned} \tag{22}$$

where $\mathcal{G}(\eta)$ is defined above. Similarly, we find that for a shifted Maxwellian

$$H_{s'}(\mathbf{v}) = \frac{n_{s'}}{v_{\mathrm{th},s'}} \mathcal{H}\left(\frac{|\mathbf{v} - \mathbf{u}_{s'}|}{v_{\mathrm{th},s'}}\right). \tag{23}$$

These results mean that we can use (20) and (21) with η defined by

$$\eta = \frac{|\mathbf{v} - \mathbf{u}_{s'}|}{v_{\mathrm{th},s'}} = \frac{\sqrt{(v_\parallel - u_{\parallel,s'})^2 + v_\perp^2}}{v_{\mathrm{th},s'}}, \tag{24}$$

where we have used that $\mathbf{u}_{s'} = u_{\parallel,s'}\mathbf{b}$ in the leading-order drift-kinetic model.

The coefficients needed for the collision operator that are derived from the Rosenbluth potentials are

$$\frac{\partial^2 G_{s'}}{\partial {v_\parallel}^2},\ \frac{\partial^2 G_{s'}}{\partial v_\parallel \partial v_\perp},\ \frac{\partial^2 G_{s'}}{\partial {v_\perp}^2},\ \frac{\partial H_{s'}}{\partial v_\parallel},\ \text{and}\ \frac{\partial H_{s'}}{\partial v_\perp}. \tag{25}$$

In terms of the functions $\mathcal{G}(\eta)$ and $\mathcal{H}(\eta)$, these coefficients are

$$\frac{\partial^2 G_{s'}}{\partial {v_\parallel}^2} = \frac{n_{s'}}{v_{\mathrm{th},s'}\eta}\left(\frac{\mathrm{d}\mathcal{G}}{\mathrm{d}\eta} + \frac{(v_\parallel - u_{\parallel,s'})^2}{v_{\mathrm{th},s'}^2}\frac{\mathrm{d}}{\mathrm{d}\eta}\left(\frac{1}{\eta}\frac{\mathrm{d}\mathcal{G}}{\mathrm{d}\eta}\right)\right), \tag{26}$$

$$\frac{\partial^2 G_{s'}}{\partial v_\parallel \partial v_\perp} = \frac{n_{s'} v_\perp (v_\parallel - u_{\parallel,s'})}{v_{\mathrm{th},s'}^3 \eta}\frac{\mathrm{d}}{\mathrm{d}\eta}\left(\frac{1}{\eta}\frac{\mathrm{d}\mathcal{G}}{\mathrm{d}\eta}\right), \tag{27}$$

$$\frac{\partial^2 G_{s'}}{\partial {v_\perp}^2} = \frac{n_{s'}}{v_{\mathrm{th},s'}\eta}\left(\frac{\mathrm{d}\mathcal{G}}{\mathrm{d}\eta} + \frac{v_\perp^2}{v_{\mathrm{th},s'}^2}\frac{\mathrm{d}}{\mathrm{d}\eta}\left(\frac{1}{\eta}\frac{\mathrm{d}\mathcal{G}}{\mathrm{d}\eta}\right)\right), \tag{28}$$

$$\frac{\partial G_{s'}}{\partial v_\perp} = \frac{n_{s'} v_\perp}{v_{\mathrm{th},s'}\eta}\frac{\mathrm{d}\mathcal{G}}{\mathrm{d}\eta}, \tag{29}$$

$$\frac{\partial H_{s'}}{\partial v_\parallel} = \frac{n_{s'}(v_\parallel - u_{\parallel,s'})}{v_{\mathrm{th},s'}^3 \eta}\frac{\mathrm{d}\mathcal{H}}{\mathrm{d}\eta}, \tag{30}$$

and

$$\frac{\partial H_{s'}}{\partial v_\perp} = \frac{n_{s'} v_\perp}{v_{\mathrm{th},s'}^3 \eta}\frac{\mathrm{d}\mathcal{H}}{\mathrm{d}\eta}, \tag{31}$$

where we have used that

$$\frac{\partial \eta}{\partial v_\parallel} = \frac{v_\parallel - u_{\parallel,s'}}{v_{\mathrm{th},s'}^2 \eta}, \quad \frac{\partial \eta}{\partial v_\perp} = \frac{v_\perp}{v_{\mathrm{th},s'}^2 \eta}. \tag{32}$$

The derivatives of $\mathcal{G}(\eta)$ and $\mathcal{H}(\eta)$ are

$$\frac{\mathrm{d}\mathcal{G}}{\mathrm{d}\eta} = \left(\frac{1}{\sqrt{\pi}}\frac{\exp\left[-\eta^2\right]}{\eta} + \left(1 - \frac{1}{2\eta^2}\right)\mathrm{erf}(\eta)\right), \tag{33}$$

$$\frac{\mathrm{d}}{\mathrm{d}\eta}\left(\frac{1}{\eta}\frac{\mathrm{d}\mathcal{G}}{\mathrm{d}\eta}\right) = \left(\left(\frac{3}{2\eta^2} - 1\right)\frac{\mathrm{erf}(\eta)}{\eta^2} - \frac{3}{\sqrt{\pi}}\frac{\exp\left[-\eta^2\right]}{\eta^3}\right), \tag{34}$$

and

$$\frac{\mathrm{d}\mathcal{H}}{\mathrm{d}\eta} = \left(\frac{2}{\sqrt{\pi}}\frac{\exp\left[-\eta^2\right]}{\eta} - \frac{\mathrm{erf}(\eta)}{\eta^2}\right) = -\frac{\mathrm{d}^2\mathcal{G}}{\mathrm{d}\eta^2}. \tag{35}$$

3.2. Collisions between Maxwellian-distributed particle species

It is tedious but straightforward to compute the fluxes for collisions between particles distributed with $F_{s'}^M$ and F_s^M. The results are

$$\Gamma_\parallel = -\frac{2}{\pi^{3/2}}\frac{\gamma_{ss'}}{m_s^2}\frac{n_{s'}n_s}{v_{\mathrm{th},s'}v_{\mathrm{th},s}^4}\exp\left[-\frac{(v_\parallel - u_{\parallel,s})^2 + v_\perp^2}{v_{\mathrm{th},s}^2}\right]\left(\frac{v_\parallel - u_{\parallel,s'}}{v_{\mathrm{th},s}}\left(\frac{\mathrm{d}^2\mathcal{G}}{\mathrm{d}\eta^2} + \frac{m_s}{m_{s'}}\frac{v_{\mathrm{th},s}^2}{v_{\mathrm{th},s'}^2}\frac{\mathrm{d}\mathcal{H}}{\mathrm{d}\eta}\right)\right.$$
$$\left. + \frac{u_{\parallel,s'} - u_{\parallel,s}}{v_{\mathrm{th},s}}\frac{1}{\eta}\left(\frac{\mathrm{d}\mathcal{G}}{\mathrm{d}\eta} + \frac{(v_\parallel - u_{\parallel,s'})^2}{v_{\mathrm{th},s'}^2}\frac{\mathrm{d}}{\mathrm{d}\eta}\left(\frac{1}{\eta}\frac{\mathrm{d}\mathcal{G}}{\mathrm{d}\eta}\right)\right)\right), \tag{36}$$

and

$$\Gamma_\perp = -\frac{2}{\pi^{3/2}}\frac{\gamma_{ss'}}{m_s^2}\frac{v_\perp n_s n_{s'}}{v_{\mathrm{th},s}^5 v_{\mathrm{th},s'}}\exp\left[-\frac{(v_\parallel - u_{\parallel,s})^2 + v_\perp^2}{v_{\mathrm{th},s}^2}\right]\left(\frac{\mathrm{d}^2\mathcal{G}}{\mathrm{d}\eta^2} + \frac{m_s}{m_{s'}}\frac{v_{\mathrm{th},s}^2}{v_{\mathrm{th},s'}^2\eta}\frac{\mathrm{d}\mathcal{H}}{\mathrm{d}\eta} + \frac{(u_{\parallel,s'} - u_{\parallel,s})(v_\parallel - u_{\parallel,s'})}{v_{\mathrm{th},s'}^2}\frac{1}{\eta}\frac{\mathrm{d}}{\mathrm{d}\eta}\left(\frac{1}{\eta}\frac{\mathrm{d}\mathcal{G}}{\mathrm{d}\eta}\right)\right), \tag{37}$$

respectively. Note that if $F_s^M = F_{s'}^M$ then $\Gamma_\parallel = \Gamma_\perp = 0$ identically.

3.3. The model Fokker-Planck operator

The numerical calculation of $G_{s'}$ from equation (12) is relatively straightforward using Clenshaw-Curtis or Gaussian quadrature integration weights. However, the integrand contains a square root function, meaning that spectrally accurate results are not guaranteed. For the Rosenbluth potential $H_{s'}$, defined by equation (13), the problem is more challenging, because the integrand diverges wherever $\mathbf{v}' = \mathbf{v}$. This problem only becomes more severe as further differentiations are applied to obtain the formal definitions of the coefficients in equation (25). Although the solution of this problem is desirable, we leave this to future work. A possible solution may be to use integration quadratures or cubatures that pack points near to the location of the divergence in $\mathbf{v}'$ (see section 19.8.6 of [10] for examples in 1D of quadratures that can resolve divergences of the form $z^{-1+\alpha}$ with z the integration variable and $\alpha > 0$). Previous authors [5, 11] have avoided this problem by using the Landau form of the collision operator, where the symmetry of the operator prevents divergences in the velocity integrals over $\mathbf{v}'$.

For this report detailing our work-in-progress, we consider the possibility of avoiding the complex integration of diverging integrands entirely. It is possible to compute the coefficients (25) by direct differentiation of $G_{s'}$, using the identity

$$\mathcal{L}\left[G_{s'}\right] = 2H_{s'}, \tag{38}$$

where the Laplacian operator is

$$\mathcal{L}\left[f\right] = \frac{\partial^2 f}{\partial {v_\parallel}^2} + \frac{1}{v_\perp}\frac{\partial}{\partial v_\perp}\left(v_\perp\frac{\partial f}{\partial v_\perp}\right). \tag{39}$$

However, up to three numerical derivatives are required to compute the coefficients (with a final fourth derivative required to evaluate the divergence of the collisional fluxes), and we find that the loss of accuracy with each numerical derivative and the initial numerical calculation of $G_{s'}$ is too high for this method to work in our current 'strong form' numerical implementation where derivatives of functions (evaluated at collocation points) are evaluated directly using interpolation with Chebyshev polynomials.

We illustrate the challenge presented by the numerical problem of computing the Rosenbluth potentials and derived coefficients using the 'strong-form' Chebyshev derivatives implemented in 'moment-kinetics'. In figure 1, we plot the maximum

absolute error in the result of calculating the Rosenbluth potential $G_{s'}$ for a Maxwellian by direct integration using equation (14), comparing to the analytical result (22). We then compute the potential $H_{s'}$ and the derived coefficients by numerical differentiation and compare the results to the analytical formulae. Note the loss of convergence with each subsequent derivative, and the deviation from the expected scaling. We can make an interesting observation by doing the same calculation for $H_{s'}$ and the derived coefficients starting from the analytically prescribed $G_{s'}$ for a Maxwellian input. The maximum errors in this calculation are shown in figure 2, demonstrating far better rates of convergence than in figure 1. (The result of computing $G_{s'}$ numerically is left on figure 2 for comparison). From this we can conclude (i) that our current scheme rapidly accrues numerical error with each subsequent derivative and (ii) the quality of the numerical integration precludes this simple 'direct' computation of the Rosenbluth potentials for arbitrary F_i. Finally, we can test the numerical implementation of the fluxes $\Gamma_{\parallel}$ and $\Gamma_{\perp}$ with the analytical results for the collisional fluxes due to colliding Maxwellian distributions. The maximum errors are shown in figure 4, demonstrating good convergence. Overall, these results demonstrate that we have implemented the collision operator correctly in our current formalism, but that the numerical methods that we are using are inadequate for the full-F operator.

To make progress towards the full Fokker Planck collision operator, whilst providing a plausible model operator, we make use of the fact that the Rosenbluth potentials are known for shifted Maxwellian distributions. Using the fact that the collision operator is bilinear, we replace the second argument $F_{s'}$ of $C_{ss'}[F_s, F_{s'}]$ with the Maxwellian distribution with the same density velocity and temperature moment $F^M_{s'}$, yielding the operator $C_{ss'}\left[F_s, F^M_{s'}\right]$ where the coefficients from the Rosenbluth potentials are given by (26)-(30). This is an uncontrolled approximation which must (eventually) be justified *a posteriori* by comparisons to results obtained using the exact collision operator. Unfortunately, we do not present simulations using this operator in this report, due to problems obtaining a stable steady-state solution. Addressing these problems are left for future work.

4. Krook operators

We now turn to a description of the Krook operator. The general Krook operator has the form

$$C^K_{ss'}[F_s, F_{s'}] = \nu_K \left(F^M_{s'}(\mathbf{v}) - F_s(\mathbf{v})\right), \tag{40}$$

where ν_K is a collision frequency, and $F^M_{s'}$ is a Maxwellian distribution formed from the first three velocity moments of $F_{s'}$, i.e.,

$$F^M_{s'}(\mathbf{v}) = \frac{n_{s'}}{\pi^{3/2} v^3_{\mathrm{th},s'}} \exp\left[-\frac{(\mathbf{v}-\mathbf{u}_{s'})^2}{v^2_{\mathrm{th},s'}}\right], \tag{41}$$

with

$$n_{s'} = \int F_{s'}(\mathbf{v}')\, d^3\mathbf{v}', \tag{42}$$

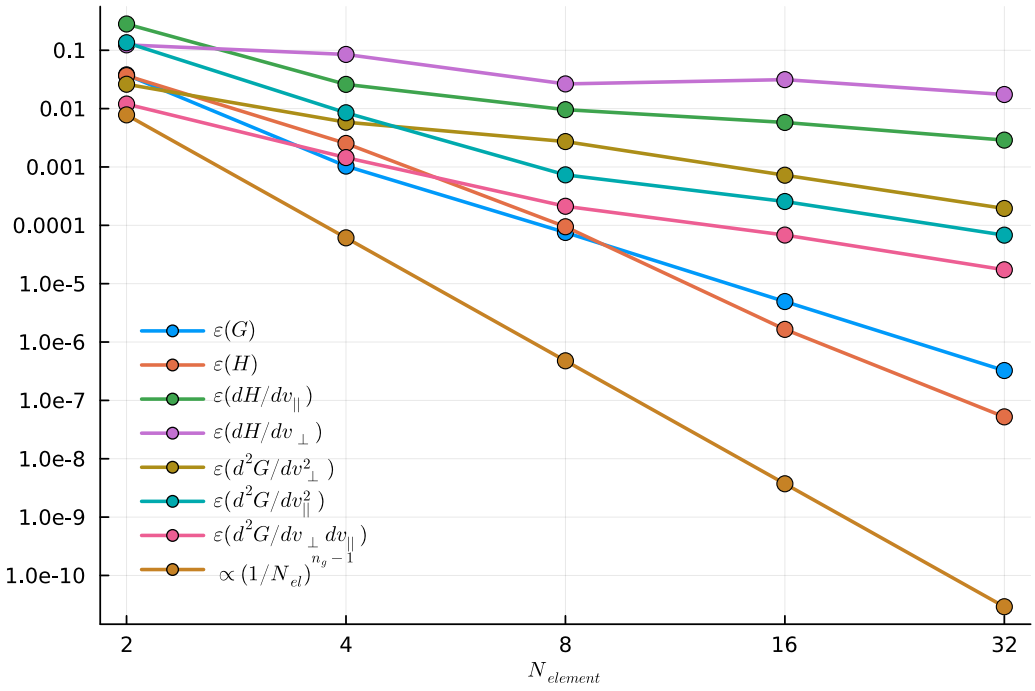

Figure 1: Results showing the numerical calculation of the Rosenbluth potential $G_{s'}$ via numerical integration, comparing to the analytical result for a shifted Maxwellian distribution. The potential $H_{s'}$ and subsequent coefficients are obtained using numerical differentiation, and compared to analytical results. The error norm is the maximum value of the absolute error. This figure was generated using the script `fkpl_test.jl` on commit `a6f06ccbbb37de8be113cb31d9c2f28c7fbdf52c`. We scan in the number of elements in the $v_{\parallel}$ and $v_{\perp}$ grids $N_{element}$, for fixed $N_{grid} = 8$, and box sizes $L_{v_{\parallel}} = 12c_{\text{ref}}$ and $L_{v_{\perp}} = 6c_{\text{ref}}$.

$$\mathbf{u}_{s'} = \frac{1}{n_{s'}} \int \mathbf{v}' F_{s'}(\mathbf{v}')\, d^3\mathbf{v}', \tag{43}$$

and

$$v_{\text{th},s'} = \sqrt{\frac{2T_{s'}}{m_{s'}}}, \text{ where } T_{s'} = \frac{m_{s'}}{3n_{s'}} \int (\mathbf{v} - \mathbf{u}_{s'})^2 F_{s'}(\mathbf{v}')\, d^3\mathbf{v}'. \tag{44}$$

We emphasise that the Krook operator is an ad-hoc model which is used primarily for simplicity when analytical calculation involving the collision operator needs to be carried out, commonly in the context of teaching pedagogical material, or when the details of the restoration of a perturbed distribution function are of no consequence.

In the drift kinetic model, this nonlinear model collision operator undergoes a simplification due to the gyrotropic nature of $F_s = F_s(v_{\parallel}, v_{\perp})$. Firstly, the leading-order mean velocity is entirely parallel to the magnetic field line, i.e.,

$$\mathbf{u}_s = u_{\parallel,s}\mathbf{b} + \mathrm{O}\left(v_{\text{th}}\rho_*\right), \tag{45}$$

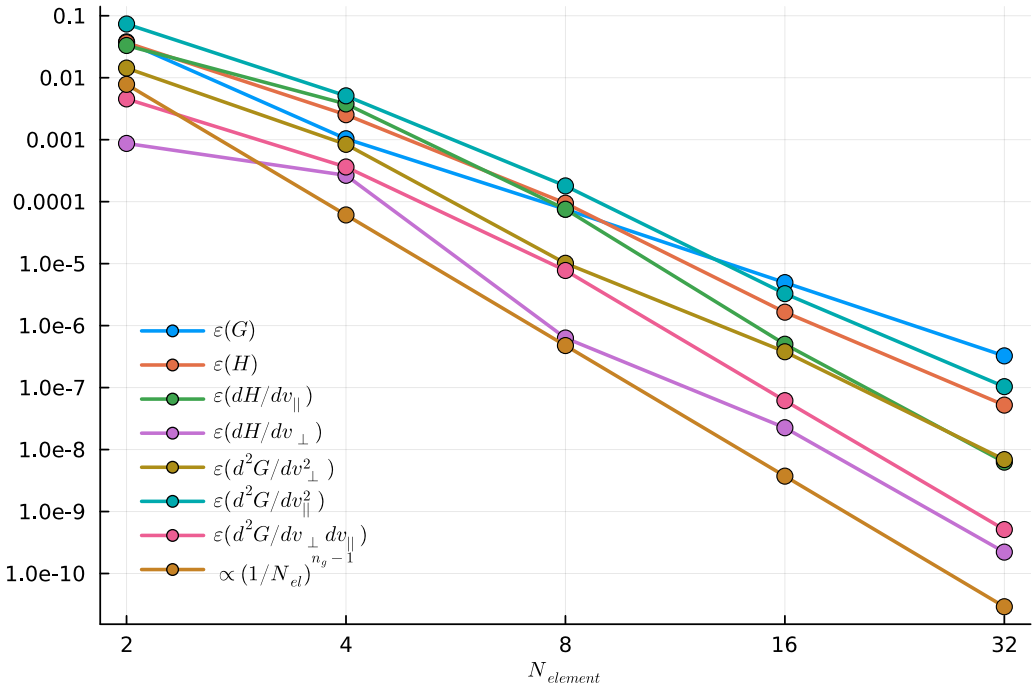

Figure 2: Results showing the numerical calculation of the Rosenbluth potential $H_{s'}$ via numerical differentiation, from an analytically specified $G_{s'}$, comparing to the analytical result for a shifted Maxwellian distribution. The subsequent coefficients are obtained using numerical differentiation of the analytically specified $G_{s'}$, and compared to analytical results. The error norm is the maximum value of the absolute error. This figure was generated using the script `fkpl_test.jl` on commit `a6f06ccbbb37de8be113cb31d9c2f28c7fbdf52c`. We scan in the number of elements in the $v_\parallel$ and $v_\perp$ grids $N_{element}$, for fixed $N_{grid} = 8$, and box sizes $L_{v_\parallel} = 12c_{\text{ref}}$ and $L_{v_\perp} = 6c_{\text{ref}}$.

with

$$u_{\parallel,s} = \frac{1}{n_s}\int_{-\infty}^{\infty}\int_{0}^{\infty} v_\parallel F_s \, 2v_\perp dv_\perp dv_\parallel. \tag{46}$$

In the model, the effect of perpendicular mean flow (the E×B flow) is only important because of the very small pitch $b_z \sim \rho_*$ of the magnetic field line. The perpendicular components of the mean flow may be found with the gyrophase-dependent part of the distribution function, which is $\mathrm{O}(\rho_*)$ small compared to F_s. Secondly, the operator appearing in the drift kinetic equation must be the gyrophase averaged Krook operator $\left\langle C^K_{ss'}[F_s, F_{s'}]\right\rangle$, where

$$\langle\cdot\rangle = \frac{1}{2\pi}\int_{-\pi}^{\pi}(\cdot)\, d\vartheta. \tag{47}$$

Using this information, we can write a more explict form of the operator that appears

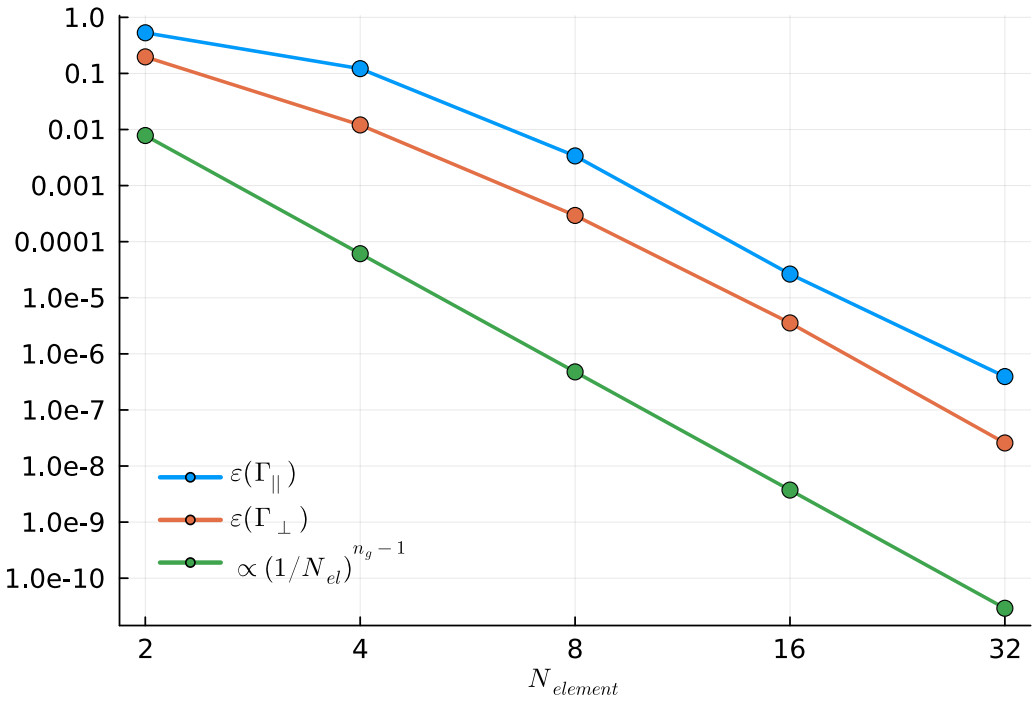

Figure 3: The result of calculating the collisional fluxes $\Gamma_{\parallel}$ and $\Gamma_{\perp}$ for Maxwellian inputs, comparing to the analytical result for differing Maxwellian distributions. The Rosenbluth potentials in these fluxes are specified analytically. The error in the calculation declines at a similar rate to the expected scaling. This figure was generated using the script `fkpl_test.jl` on commit `a6f06ccbbb37de8be113cb31d9c2f28c7fbdf52c`. We scan in the number of elements in the $v_{\parallel}$ and $v_{\perp}$ grids $N_{element}$, for fixed $N_{grid} = 8$, and box sizes $L_{v_{\parallel}} = 12c_{\mathrm{ref}}$ and $L_{v_{\perp}} = 6c_{\mathrm{ref}}$.

in the drift kinetic equation, to leading-order in $\mathrm{O}(\rho_*)$:

$$\left\langle C^K_{ss'}\left[F_s, F_{s'}\right]\right\rangle = \nu_K \left(\frac{n_{s'}}{\pi^{3/2} v^3_{\mathrm{th},s'}} \exp\left[-\frac{\left(v_{\parallel} - u_{\parallel,s'}\right)^2 + v_{\perp}^2}{v^2_{\mathrm{th},s'}} \right] - F_s(v_{\parallel}, v_{\perp}) \right). \tag{48}$$

5. Normalised system of equations

The normalised drift kinetic equation for ions may be written as

$$\begin{aligned} \frac{\partial \widetilde{F}_i}{\partial \tilde{t}} + b_z \tilde{v}_{\parallel} \frac{\partial \widetilde{F}_i}{\partial \tilde{z}} + \frac{b_z \widetilde{E}_z}{2} \frac{\partial \widetilde{F}_i}{\partial \tilde{v}_{\parallel}} = \\ \widetilde{C}_{ii}\left[\widetilde{F}_i, \widetilde{F}_i^M\right] + \tilde{\nu}_K \left(\widetilde{F}_i^M - \widetilde{F}_i\right) + \tilde{\nu}_{\parallel} \frac{\partial^2 \widetilde{F}_i}{\partial \tilde{v}_{\parallel}^2} + \widetilde{S}_i, \end{aligned} \tag{49}$$

where $c_{\mathrm{ref}} = \sqrt{2T_{\mathrm{ref}} m_{\mathrm{ref}}}$ is the normalising speed and L_{ref} is the normalising length. The variables $\tilde{t} = tc_{\mathrm{ref}}/L_{\mathrm{ref}}$, $\tilde{v}_{\parallel} = v_{\parallel}/c_{\mathrm{ref}}$, $\tilde{v}_{\perp} = v_{\perp}/c_{\mathrm{ref}}$, $\tilde{z} = z/L_{\mathrm{ref}}$. The normalised

distribution functions are $\widetilde{F}_i = \pi^{3/2} c_{\rm ref}^3 F_i / n_{\rm ref}$, with $n_{\rm ref}$ the normalising density. The normalised diffusion coefficient $\tilde{\nu}_\parallel = L_{\rm ref}\nu_\parallel / c_{\rm ref}^3$. The normalised source is $\widetilde{S}_i = L_{\rm ref} S_i / c_{\rm ref}$, the normalised Krook operator frequency is $\tilde{\nu}_K = L_{\rm ref}\nu_K / c_{\rm ref}$. The potential $\widetilde{\phi} = e\phi / T_{\rm ref}$ is determined by the normalised quasineutrality relation,

$$\widetilde{n}_i = \widetilde{n}_e = \widetilde{N}_e \exp\left(\frac{\widetilde{\phi}}{\widetilde{T}_e}\right). \tag{50}$$

The normalised electric fields are defined by

$$\widetilde{E}_z = -\frac{\partial \widetilde{\phi}}{\partial \tilde{z}}, \text{ and } \quad \widetilde{E}_r = -\frac{\partial \widetilde{\phi}}{\partial \tilde{r}}. \tag{51}$$

and the density is defined by

$$\widetilde{n}_i = \frac{1}{\sqrt{\pi}} \int_{-\infty}^{\infty} d\tilde{v}_\parallel \int_0^{\infty} 2 d\tilde{v}_\perp \tilde{v}_\perp \widetilde{F}_i. \tag{52}$$

The normalised Maxwellian distribution $\widetilde{F}_i^M$ is defined by setting $s' = i$ in the following expression,

$$\widetilde{F}_{s'}^M = \frac{\tilde{n}_{s'}}{\tilde{v}_{{\rm th},s'}^3} \exp\left[-\frac{\left(\tilde{v}_\parallel - \tilde{u}_{\parallel,s'}\right)^2 + \tilde{v}_\perp^2}{\tilde{v}_{{\rm th},s'}^2}\right] \tag{53}$$

with $\tilde{n}_{s'} = n_{s'}/n_{\rm ref}$, $\tilde{v}_{{\rm th},s'} = v_{{\rm th},s'}/c_{\rm ref}$, and $\tilde{u}_{\parallel,s'} = u_{\parallel,s}/c_{\rm ref}$.

Finally, the normalised Fokker-Planck operator is given by

$$\widetilde{C}_{ss'}\left[\widetilde{F}_s, \widetilde{F}_{s'}\right] = \frac{\partial \widetilde{\Gamma}_\parallel}{\partial \tilde{v}_\parallel} + \frac{1}{\tilde{v}_\perp}\frac{\partial}{\partial \tilde{v}_\perp}\left(\tilde{v}_\perp \widetilde{\Gamma}_\perp\right), \tag{54}$$

with

$$\widetilde{\Gamma}_\parallel = \widetilde{\nu}_{ss'}\left(\frac{\partial \widetilde{F}_s}{\partial \tilde{v}_\parallel}\frac{\partial^2 \widetilde{G}_{s'}}{\partial \tilde{v}_\parallel^2} + \frac{\partial \widetilde{F}_s}{\partial \tilde{v}_\perp}\frac{\partial^2 \widetilde{G}_{s'}}{\partial \tilde{v}_\perp \partial \tilde{v}_\parallel} - 2\frac{m_s}{m_{s'}} F_s \frac{\partial \widetilde{H}_{s'}}{\partial \tilde{v}_\parallel}\right), \tag{55}$$

and

$$\widetilde{\Gamma}_\perp = \widetilde{\nu}_{ss'}\left(\frac{\partial \widetilde{F}_s}{\partial \tilde{v}_\parallel}\frac{\partial^2 \widetilde{G}_{s'}}{\partial \tilde{v}_\parallel \partial \tilde{v}_\perp} + \frac{\partial \widetilde{F}_s}{\partial \tilde{v}_\perp}\frac{\partial^2 \widetilde{G}_{s'}}{\partial \tilde{v}_\perp^2} - 2\frac{m_s}{m_{s'}} \widetilde{F}_s \frac{\partial \widetilde{H}_{s'}}{\partial \tilde{v}_\perp}\right), \tag{56}$$

where $\widetilde{\nu}_{ss'} = L_{\rm ref}\nu_{ss'}/c_{\rm ref}$ and

$$\nu_{ss'} = \frac{\gamma_{ss'} n_{\rm ref}}{m_s^2 c_{\rm ref}^3}. \tag{57}$$

The normalised Rosenbluth potentials are defined by

$$G_{s'} = n_{\rm ref} c_{\rm ref} \widetilde{G}_{s'}, \text{ and } \quad H_{s'} = \frac{n_{\rm ref}}{c_{\rm ref}} \widetilde{H}_{s'}. \tag{58}$$

with integral definitions given by

$$\widetilde{G}_{s'} = \int_0^{\infty}\int_{-\infty}^{\infty} \left(\left(\tilde{v}_\parallel - \tilde{v}'_\parallel\right)^2 + \left(\tilde{v}_\perp + \tilde{v}'_\perp\right)^2\right)^{1/2} \frac{2E(k(\tilde{v}_\parallel, \tilde{v}_\perp, \tilde{v}'_\parallel, \tilde{v}'_\perp))}{\pi} \widetilde{F}_{s'}(\tilde{v}'_\parallel, \tilde{v}'_\perp) \frac{2\tilde{v}'_\perp}{\sqrt{\pi}}\, d\tilde{v}'_\parallel d\tilde{v}'_\perp \tag{59}$$

and

$$\widetilde{H}_{s'} = \int_0^\infty \int_{-\infty}^\infty \left(\left(\tilde{v}_\parallel - \tilde{v}'_\parallel\right)^2 + \left(\tilde{v}_\perp + \tilde{v}'_\perp\right)^2 \right)^{-1/2} \frac{2K(k(\tilde{v}_\parallel, \tilde{v}_\perp, \tilde{v}'_\parallel, \tilde{v}'_\perp))}{\pi} \widetilde{F}_{s'}(\tilde{v}'_\parallel, \tilde{v}'_\perp) \frac{2\tilde{v}'_\perp}{\sqrt{\pi}}\, d\tilde{v}'_\parallel d\tilde{v}'_\perp, \tag{60}$$

respectively. The normalised values of the Rosenbluth potential coefficients for a shifted Maxwellian may be inferred from equations (26)-(30) and (58).

5.1. Calculating the thermal speed

To evaluate the Krook operator, we must calculate the thermal speed. We normalise the velocities to $c_{\rm ref} = \sqrt{2T_{\rm ref}/m_{\rm ref}}$. Hence, the normalised thermal speed is

$$\tilde{v}_{{\rm th},s} = \frac{v_{{\rm th},s}}{c_{\rm ref}} = \sqrt{\frac{T_s}{T_{\rm ref}} \frac{m_{\rm ref}}{m_s}} = \sqrt{\frac{\tilde{T}_s}{\tilde{m}_s}}. \tag{61}$$

We calculate the normalised temperature from the pressure and the density. The isotropic pressure is defined by

$$p_s = \frac{m_s}{3} \int_{-\infty}^\infty \int_0^\infty \left((v'_\parallel - u_{\parallel,s})^2 + (v'_\perp)^2 \right) F_s(v'_\parallel, v'_\perp)\, 2\pi v'_\perp dv'_\perp dv'_\parallel. \tag{62}$$

The normalised pressure $\tilde{p}_s = p_s/n_{\rm ref}T_{\rm ref}$ is then given by

$$\tilde{p}_s = \frac{2\tilde{m}_s}{3} \int_{-\infty}^\infty \int_0^\infty \left((\tilde{v}'_\parallel - \tilde{u}_{\parallel,s})^2 + (\tilde{v}'_\perp)^2 \right) \widetilde{F}_s(\tilde{v}'_\parallel, \tilde{v}'_\perp)\, \frac{2\tilde{v}'_\perp}{\sqrt{\pi}} d\tilde{v}'_\perp d\tilde{v}'_\parallel. \tag{63}$$

We can also define a parallel pressure

$$p_{\parallel,s} = m_s \int_{-\infty}^\infty \int_0^\infty (v'_\parallel - u_{\parallel,s})^2 F_s(v'_\parallel, v'_\perp)\, 2\pi v'_\perp dv'_\perp dv'_\parallel, \tag{64}$$

and a perpendicular pressure

$$p_{\perp,s} = \frac{m_s}{2} \int_{-\infty}^\infty \int_0^\infty (v'_\perp)^2 F_s(v'_\parallel, v'_\perp)\, 2\pi v'_\perp dv'_\perp dv'_\parallel, \tag{65}$$

so that

$$p_s = \frac{1}{3} \left(p_{\parallel,s} + 2p_{\perp,s} \right). \tag{66}$$

The normalised parallel and perpendicular pressures $\tilde{p}_{\parallel,s} = p_{\parallel,s}/n_{\rm ref}T_{\rm ref}$ and $\tilde{p}_{\perp,s} = p_{\perp,s}/n_{\rm ref}T_{\rm ref}$ are

$$\tilde{p}_{\parallel,s} = 2\tilde{m}_s \int_{-\infty}^\infty \int_0^\infty (\tilde{v}'_\parallel - \tilde{u}_{\parallel,s})^2 \widetilde{F}_s(\tilde{v}'_\parallel, \tilde{v}'_\perp)\, \frac{2v'_\perp}{\sqrt{\pi}} d\tilde{v}'_\perp d\tilde{v}'_\parallel, \tag{67}$$

and

$$\tilde{p}_{\perp,s} = \tilde{m}_s \int_{-\infty}^\infty \int_0^\infty (\tilde{v}'_\perp)^2 \widetilde{F}_s(\tilde{v}'_\parallel, \tilde{v}'_\perp)\, \frac{2v'_\perp}{\sqrt{\pi}} d\tilde{v}'_\perp d\tilde{v}'_\parallel, \tag{68}$$

respectively. Finally, we use that $\tilde{T}_s = T_s/T_{\rm ref} = p_s/n_s T_{\rm ref} = \tilde{p}_s/\widetilde{n}_s$ to write

$$\tilde{v}_{{\rm th},s} = \sqrt{\frac{\tilde{p}_s}{\tilde{m}_s \widetilde{n}_s}} \tag{69}$$

5.2. Extending the wall-boundary manufactured solutions test results

To test the implementation of the Krook operator, we require results for the plasma density, velocity, and thermal speed. We calculate these quantities in the existing wall-boundary test existing in the moment-kinetics code framework [12]. For the distribution function, we choose

$$\widetilde{F}_i = \Bigg[H\left(\overline{v}_\parallel\right)\overline{v}_\parallel^4\left(\frac{1}{2}+\frac{\tilde{z}}{\tilde{L}_z}\right)n_+(\tilde{z},\tilde{r}) + H\left(-\overline{v}_\parallel\right)\overline{v}_\parallel^4\left(\frac{1}{2}-\frac{\tilde{z}}{\tilde{L}_z}\right)n_-(\tilde{z},\tilde{r}) + \left(\frac{1}{2}-\frac{\tilde{z}}{\tilde{L}_z}\right)\left(\frac{1}{2}+\frac{\tilde{z}}{\tilde{L}_z}\right)n_0(\tilde{z},\tilde{r})\Bigg]\exp\left(-\overline{v}_\parallel^2-\tilde{v}_\perp^2\right), \tag{70}$$

where $\overline{v}_\parallel = \tilde{v}_\parallel - \alpha\rho_*\widetilde{E}_r/2b_z$, and α takes the values of 0 or 1 depending on the type of test carried out. We require the forms of $\widetilde{n}_i$, $\widetilde{u}_{\parallel i}$, $\widetilde{p}_{\parallel i}$ and $\widetilde{p}_{\perp i}$. We assume that $\tilde{m}_\mathrm{i} = 1$.

The normalised ion density is defined by

$$\widetilde{n}_i = \frac{1}{\sqrt{\pi}}\int_{-\infty}^{\infty} d\tilde{v}_\parallel \int_0^\infty 2d\tilde{v}_\perp\tilde{v}_\perp\widetilde{F}_i. \tag{71}$$

Evaluating this integral, we find that

$$\widetilde{n}_i = \frac{3}{8}n_+(\tilde{z},\tilde{r})\left(\frac{1}{2}+\frac{\tilde{z}}{\tilde{L}_z}\right) + \frac{3}{8}n_-(\tilde{z},\tilde{r})\left(\frac{1}{2}-\frac{\tilde{z}}{\tilde{L}_z}\right) + n_0(\tilde{z},\tilde{r})\left(\frac{1}{2}+\frac{\tilde{z}}{\tilde{L}_z}\right)\left(\frac{1}{2}-\frac{\tilde{z}}{\tilde{L}_z}\right). \tag{72}$$

The normalised velocity is defined by

$$\begin{aligned}\widetilde{n}_i\widetilde{u}_{\parallel i} &= \frac{1}{\sqrt{\pi}}\int_{-\infty}^{\infty} d\tilde{v}_\parallel\int_0^\infty 2d\tilde{v}_\perp\tilde{v}_\perp\tilde{v}_\parallel\widetilde{F}_i \\ &= \frac{1}{\sqrt{\pi}}\int_{-\infty}^{\infty} d\overline{v}_\parallel\int_0^\infty 2d\tilde{v}_\perp\tilde{v}_\perp\left(\overline{v}_\parallel+\frac{\alpha\rho_*\widetilde{E}_r}{2b_z}\right)\widetilde{F}_i.\end{aligned} \tag{73}$$

We evaluate this integral to find that

$$\widetilde{n}_i\widetilde{u}_{\parallel i} = \frac{1}{\sqrt{\pi}}\left(n_+(\tilde{z},\tilde{r})\left(\frac{1}{2}+\frac{\tilde{z}}{\tilde{L}_z}\right) - n_-(\tilde{z},\tilde{r})\left(\frac{1}{2}-\frac{\tilde{z}}{\tilde{L}_z}\right)\right) + \widetilde{n}_i\frac{\alpha\rho_*\widetilde{E}_r}{2b_z}. \tag{74}$$

The normalised parallel pressure is

$$\begin{aligned}\widetilde{p}_{\parallel i} &= 2\int_{-\infty}^{\infty}\int_{0}^{\infty}(\tilde{v}'_{\parallel}-\widetilde{u}_{\parallel i})^2\widetilde{F}_i(\tilde{v}'_{\parallel},\tilde{v}'_{\perp})\,\frac{2v'_{\perp}}{\sqrt{\pi}}d\tilde{v}'_{\perp}d\tilde{v}'_{\parallel}\\ &= 2\int_{-\infty}^{\infty}\int_{0}^{\infty}\left(\overline{v}_{\parallel}+\frac{\alpha\rho_*\widetilde{E}_r}{2b_z}-\widetilde{u}_{\parallel i}\right)^2\widetilde{F}_i(\tilde{v}'_{\parallel}(\overline{v}_{\parallel}),\tilde{v}'_{\perp})\,\frac{2v'_{\perp}}{\sqrt{\pi}}d\tilde{v}'_{\perp}d\overline{v}_{\parallel}\\ &= 2\int_{-\infty}^{\infty}\int_{0}^{\infty}\left(\overline{v}_{\parallel}^2+2\overline{v}_{\parallel}\left(\frac{\alpha\rho_*\widetilde{E}_r}{2b_z}-\widetilde{u}_{\parallel i}\right)+\left(\frac{\alpha\rho_*\widetilde{E}_r}{2b_z}-\widetilde{u}_{\parallel i}\right)^2\right)\widetilde{F}_i(\tilde{v}'_{\parallel}(\overline{v}_{\parallel}),\tilde{v}'_{\perp})\,\frac{2v'_{\perp}}{\sqrt{\pi}}d\tilde{v}'_{\perp}d\overline{v}_{\parallel}\\ &= 2\int_{-\infty}^{\infty}\int_{0}^{\infty}\overline{v}_{\parallel}^2\widetilde{F}_i(\tilde{v}'_{\parallel}(\overline{v}_{\parallel}),\tilde{v}'_{\perp})\,\frac{2v'_{\perp}}{\sqrt{\pi}}d\tilde{v}'_{\perp}d\overline{v}_{\parallel}-2\widetilde{n}_i\left(\frac{\alpha\rho_*\widetilde{E}_r}{2b_z}-\widetilde{u}_{\parallel i}\right)^2\end{aligned} \tag{75}$$

Evaluating the final Gaussian integral, we have that

$$\begin{aligned}\widetilde{p}_{\parallel i} =&\frac{15}{8}n_+(\tilde{z},\tilde{r})\left(\frac{1}{2}+\frac{\tilde{z}}{\tilde{L}_z}\right)+\frac{15}{8}n_-(\tilde{z},\tilde{r})\left(\frac{1}{2}-\frac{\tilde{z}}{\tilde{L}_z}\right)\\ &+n_0(\tilde{z},\tilde{r})\left(\frac{1}{2}+\frac{\tilde{z}}{\tilde{L}_z}\right)\left(\frac{1}{2}-\frac{\tilde{z}}{\tilde{L}_z}\right)-2\widetilde{n}_i\left(\frac{\alpha\rho_*\widetilde{E}_r}{2b_z}-\widetilde{u}_{\parallel i}\right)^2.\end{aligned} \tag{76}$$

We can write the final term on the RHS explicitly as

$$\begin{aligned}\widetilde{p}_{\parallel i} =&\frac{15}{8}n_+(\tilde{z},\tilde{r})\left(\frac{1}{2}+\frac{\tilde{z}}{\tilde{L}_z}\right)+\frac{15}{8}n_-(\tilde{z},\tilde{r})\left(\frac{1}{2}-\frac{\tilde{z}}{\tilde{L}_z}\right)+n_0(\tilde{z},\tilde{r})\left(\frac{1}{2}+\frac{\tilde{z}}{\tilde{L}_z}\right)\left(\frac{1}{2}-\frac{\tilde{z}}{\tilde{L}_z}\right)\\ &-\frac{2}{\pi\widetilde{n}_i}\left(n_+(\tilde{z},\tilde{r})\left(\frac{1}{2}+\frac{\tilde{z}}{\tilde{L}_z}\right)-n_-(\tilde{z},\tilde{r})\left(\frac{1}{2}-\frac{\tilde{z}}{\tilde{L}_z}\right)\right)^2.\end{aligned} \tag{77}$$

Finally, the normalised perpendicular pressure is

$$\widetilde{p}_{\perp i} = \int_{-\infty}^{\infty}\int_{0}^{\infty}(\tilde{v}'_{\perp})^2\widetilde{F}_i(\tilde{v}'_{\parallel},\tilde{v}'_{\perp})\,\frac{2v'_{\perp}}{\sqrt{\pi}}d\tilde{v}'_{\perp}d\tilde{v}'_{\parallel}, \tag{78}$$

and we evaluate this integral to find that

$$\widetilde{p}_{\perp i} = \widetilde{n}_i. \tag{79}$$

5.3. A convergence test in 1D2V

To demonstrate the correct implementation of the Krook collision operator in two velocity dimensions, we use the analytical results derived in the previous section to carry out a manufactured solutions test. For the physical parameters in the model, we take $b_z = 1.0$, $\tilde{\nu}_K = 1.0$, $\tilde{\nu}_{\parallel} = 0.0$, $\widetilde{\nu}_{ii} = 0.0$, $\widetilde{N}_e = 1.0$, and $\widetilde{T}_e = 1.0$. The input file corresponding to these parameters is given in section Appendix A.1. To test the convergence, we carry out the simulation until $\tilde{t} = 1$, for varying number

of elements $N_{element}$ in each of the coordinate dimensions z, $v_\parallel$, and $v_\perp$. The number of points per element is taken to be $N_{grid} = 17$, with $L_{v_\parallel} = 2L_{v_\perp} = 12c_{\text{ref}}$. We take $\Delta\tilde{t} = 0.002/N_{element}$. The results of the scan are shown in figure 4, where the error norms plotted are the average RMS values (see equations (10)-(13) of [12]). The expected scaling is plotted. We note that the convergence is slower than the expected scaling, but still good, albeit with a rollover at the very largest values of $N_{element}$. We take these results to indicate that we have correctly implemented the Krook operator. The simulations were carried out with commit `a6f06ccbbb37de8be113cb31d9c2f28c7fbdf52c`.

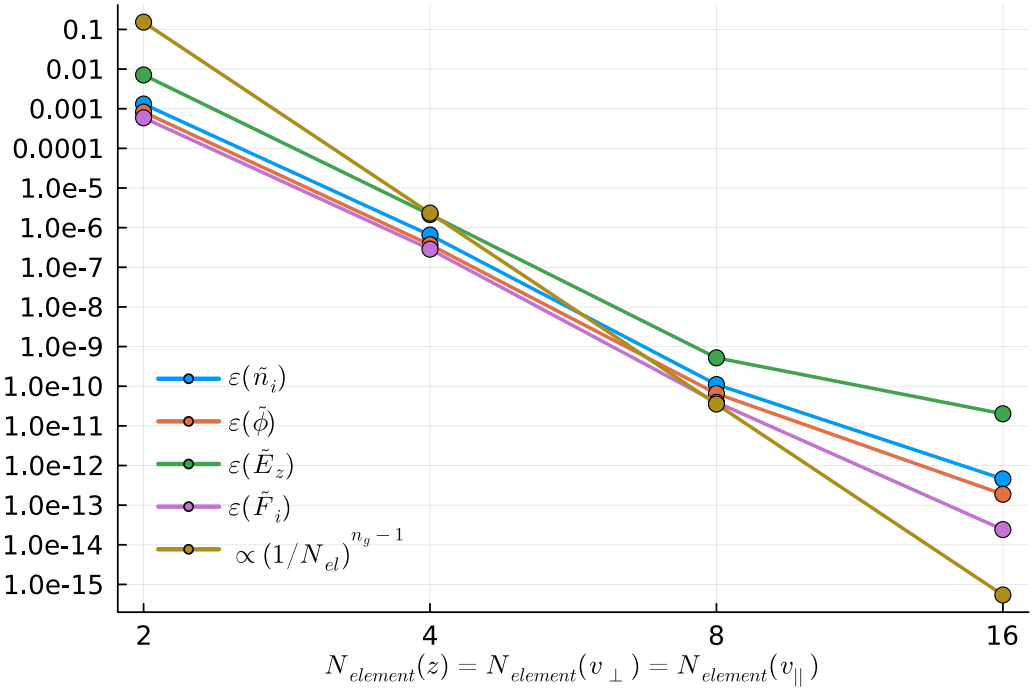

Figure 4: Results demonstrating the correct implementation of the Krook collision operator $\tilde{\nu}_K(\widetilde{F}_i^M - \widetilde{F}_i)$, in a case with wall boundary conditions. The input file corresponding to these simulations is given in section Appendix A.1. Here, $N_{el} = N_{element}$ and $n_g = N_{grid}$.

6. Steady-state solutions with a Krook collision operator

In this section, we examine the behaviour of the sheath model in the presence of a simple ionisation source

$$\widetilde{S}_i = \exp\left[-\tilde{v}_\parallel^2 - \tilde{v}_\perp^2\right], \tag{80}$$

and the Krook operator and numerical dissipation. We use the manufactured solution as an initial condition, and we allow the system to relax to a steady state. We will see that a larger Krook collision frequency $\tilde{\nu}_K$ forces the distribution function to be

broader in velocity space, including at the sheath entrance near the wall. For the physics parameters, we take $b_z = 1.0$, $\tilde{\nu}_{\parallel} = 0.01$, $\widetilde{\nu}_{ii} = 0.0$ $\widetilde{N}_e = 1.0$, and $\widetilde{T}_e = 1.0$. We will vary $\tilde{\nu}_K$ between 10 and 0.01. The input file corresponding to these simulations is given in section Appendix A.2.For the numerical input values we take $N_{grid} = 17$ for all dimensions, $N_{element} = 8$ for $v_{\parallel}$ and $v_{\perp}$ dimensions and $N_{element} = 9$ for the z dimension. We do this to avoid having the point $z = 0$ $v_{\parallel} = 0$ on grid, as this point is a stagnation point in this model for an up-down symmetric simulation. We take $L_{v_{\parallel}} = 2L_{v_{\perp}} = 6$.

6.1. Krook plus numerical diffusion

First, we examine in detail a simulation where we take $\tilde{\nu}_K = 0.1$. After running to a time of $\tilde{t} = 10$ with a timestep of $\Delta\tilde{t} = 0.0005$, we find the potential, electric field, and distribution function visualised in figure 5. In figure 5a we plot the potential $\widetilde{\phi}$, and in figure 5b we plot the electric field $\widetilde{E}_z$. These fields show the expected sheath-like behaviour with a diverging electric field near the sheath entrances at $z/L_z = \pm 1/2$. In figures 5c and 5d we visualise the velocity space structure of the distribution at $z/L_z = -1/2$. In figure 5e we show the structure of the distribution function at a typical $v_{\perp}$ as a function of $\tilde{z}$ and $\tilde{v}_{\parallel}$. Finally, in figure 5f we show the mean velocity $\widetilde{u}_{\parallel i}$.

6.2. Varying the strength of the Krook operator

We illustrate the impact on the solution of including a Krook collision operator in figure 6. By varying the Krook collision frequency $\tilde{\nu}_K$ from 0.01 to 10.0, we can change the extent of the distribution function in velocity space. This behaviour comes about because the Krook operator attempts to force the ion distribution function towards a shifted Maxwellian. It is interesting to note that although the ionisation source (80) is Maxwellian (with no mean flow), the ion distribution function is not close to Maxwellian as the ions approach the sheath, even in the presence of the Krook operator.

7. Discussion

This report has investigated the (work-in-progress) implementation of ion-ion collision operators into the 'moment-kinetics' code. We have reported on two lines of development: a successful implementation of a Krook operator; and initial investigation into the application of the numerical methods currently used by the 'moment-kinetics' code to the implemention of the exact Fokker-Planck collision operator. We developed a series of tests to test the calculation of the coefficients and fluxes appearing in the Fokker-Planck collision operator. We found that special quadratures that can handle divergences in the integrand may be required to compute the coefficients appearing in the Fokker-Planck operator, and that repeated differentiation can lead to inaccurate results in our implementation.

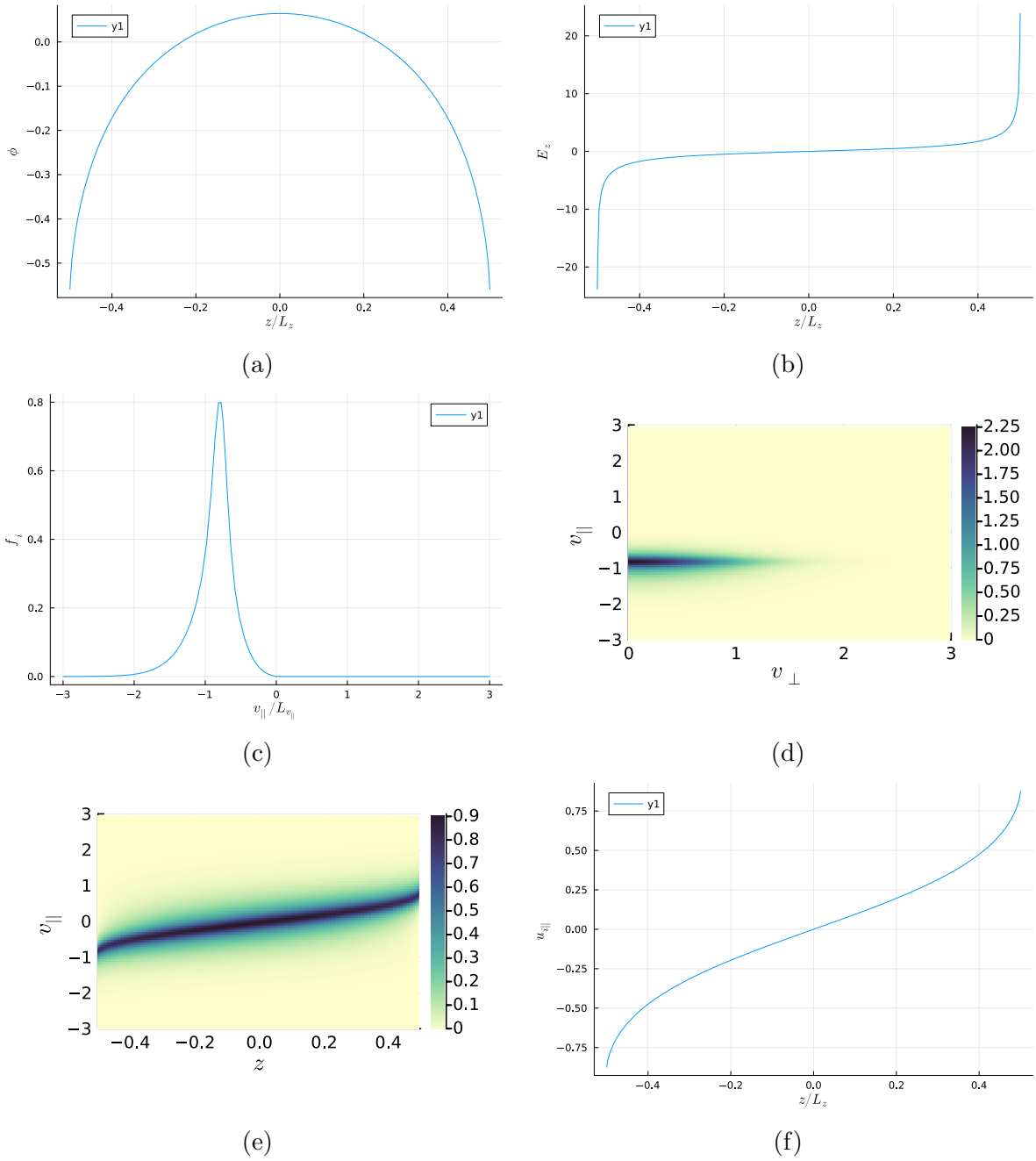

Figure 5: The relaxed state of simulating equation (49) with the source (80) and a Krook operator with $\tilde{\nu}_K = 0.1$. Numerical dissipation is included with $\nu_\parallel = 0.01$. We take $\widetilde{\nu}_{ii} = 0.0$

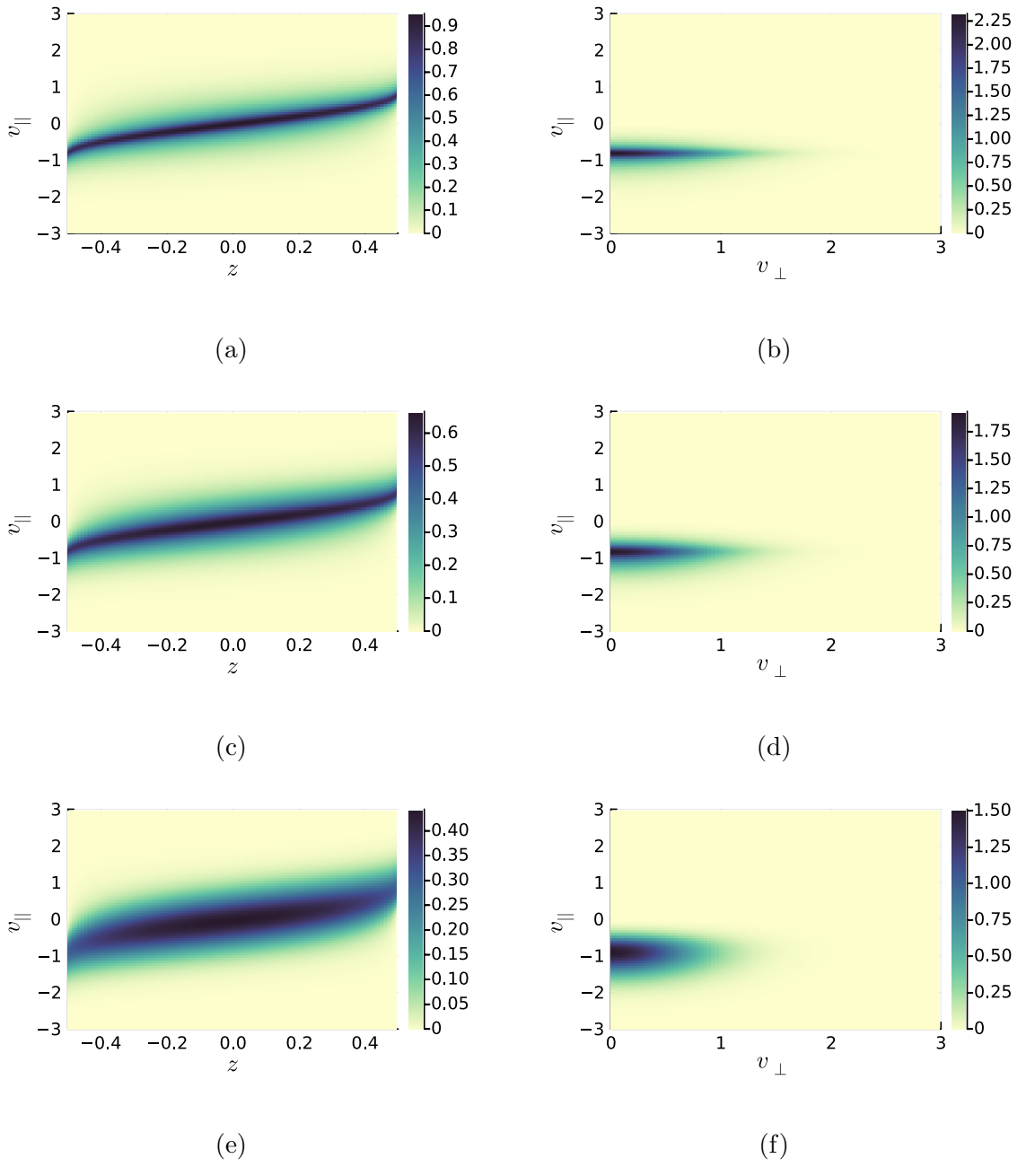

Figure 6: The distribution function as a function of z and $v_\parallel$ (at a typical $v_\perp$) and at the sheath entrane at $zL_z = -1/2$ as a function of $v_\parallel$ and $v_\perp$. Taken from the relaxed state found by simulating equation (49) with the source (80) and a Krook operator with $\tilde{\nu}_K = 0.01$ (6a and 6b), $\tilde{\nu}_K = 1.0$ (6c and 6d), and $\tilde{\nu}_K = 10.0$ (6e and 6f). Numerical dissipation is included with $\nu_\parallel = 0.01$. We take $\widetilde{\nu}_{ii} = 0.0$.

To avoid the numerical integration required for the full Fokker-Planck operator, we investigated the possibility of implementing a modified collision operator which leverages the analytical results for the Rosenbluth potentials for a shifted Maxwellian. This operator was tested, demonstrating a likely correct implementation. However, steady-state solutions obtained with this operator are currently difficult to obtain. At the time of writing this report, the modified Fokker-Planck operator tends to produce distribution functions which go negative with Gibbs phenomena in the long time limit, suggesting numerical issues, or a bug.

Because the Fokker-Planck collision operator represents the gold standard, and all model operators are simply ad hoc prescriptions made via uncontrolled approximations, it is highly desirable to have the proper Fokker-Planck operator implemented. This report highlights the need to consider other numerical methods which might allow us to compute the Rosenbluth potentials accurately, or otherwise implement the operator. Quadratures that can handle certain types of diverging integrands do exist, as mentioned in section 19.8.6 of [10]. Previous implementations of the full Fokker-Planck operator exist in the literature, suggesting several methods to approach the problem [13, 14, 11, 5]. An obvious route to follow is to use the weak formulation of the problem, to use integration by parts to reduce the order of the derivatives formally required in the numerical differentiation. Another option could be to focus on the Landau form of the Fokker Planck operator rather than on on the Rosenbluth-MacDonald-Judd form, see e.g., [5, 11]. Further work will attempt to determine whether or not the weak formulation provides any advantages in our framework.

Appendix A. Input data

In this appendix we give simulation inputs to be used with the 'moment kinetics' branch `https://github.com/mabarnes/moment_kinetics/tree/radial-vperp-standard-DKE-Julia-1.7.2-mpi`. on commit `a6f06ccbbb37de8be113cb31d9c2f28c7fbdf52c`.

Appendix A.1. Simulation input: MMS test with a Krook operator

```
use_manufactured_solns_for_advance = true
n_ion_species = 1
n_neutral_species = 0
electron_physics = "boltzmann_electron_response"
#electron_physics = "boltzmann_electron_response_with_simple_sheath"
run_name = "1D-wall_MMS_nel_r_1_z_8_vpa_8_vperp_8_krook"
evolve_moments_density = false
evolve_moments_parallel_flow = false
evolve_moments_parallel_pressure = false
evolve_moments_conservation = false
force_Er_zero_at_wall = false #true
```

```
Er_constant = 0.0
epsilon_offset = 0.1
use_vpabar_in_mms_dfni = true
T_e = 1.0
T_wall = 1.0
rhostar = 1.0
Bzed = 1.0
Bmag = 1.0
initial_density1 = 0.5
initial_temperature1 = 1.0
initial_density2 = 0.5
initial_temperature2 = 1.0
z_IC_option1 = "sinusoid"
z_IC_density_amplitude1 = 0.001
z_IC_density_phase1 = 0.0
z_IC_upar_amplitude1 = 0.0
z_IC_upar_phase1 = 0.0
z_IC_temperature_amplitude1 = 0.0
z_IC_temperature_phase1 = 0.0
z_IC_option2 = "sinusoid"
z_IC_density_amplitude2 = 0.001
z_IC_density_phase2 = 0.0
z_IC_upar_amplitude2 = 0.0
z_IC_upar_phase2 = 0.0
z_IC_temperature_amplitude2 = 0.0
z_IC_temperature_phase2 = 0.0
charge_exchange_frequency = 0.0
ionization_frequency = 0.0
nuii_krook = 1.0
nstep = 4000
dt = 0.00025
nwrite = 400
nwrite_dfns = 400
use_semi_lagrange = false
n_rk_stages = 4
split_operators = false
z_ngrid = 17
z_nelement = 8
z_nelement_local = 8
z_bc = "wall"
z_discretization = "chebyshev_pseudospectral"
r_ngrid = 1
```

```
r_nelement = 1
r_nelement_local = 1
r_bc = "periodic"
r_discretization = "chebyshev_pseudospectral"
vpa_ngrid = 17
vpa_nelement = 8
vpa_L = 12.0
vpa_bc = "zero"
vpa_discretization = "chebyshev_pseudospectral"
vperp_ngrid = 17
vperp_nelement = 8
vperp_L = 6.0
vperp_bc = "periodic"
#vperp_discretization = "finite_difference"
vperp_discretization = "chebyshev_pseudospectral"

vz_ngrid = 17
vz_nelement = 4
vz_L = 12.0
vz_bc = "periodic"
vz_discretization = "chebyshev_pseudospectral"

vr_ngrid = 17
vr_nelement = 4
vr_L = 12.0
vr_bc = "periodic"
vr_discretization = "chebyshev_pseudospectral"

vzeta_ngrid = 17
vzeta_nelement = 4
vzeta_L = 12.0
vzeta_bc = "periodic"
vzeta_discretization = "chebyshev_pseudospectral"

[numerical_dissipation]
vpa_dissipation_coefficient = 0.0
#z_dissipation_coefficient = 0.1
r_dissipation_coefficient = 0.0
```

Appendix A.2. Simulation input: steady-state runs with a Krook operator

```
use_manufactured_solns_for_init = true
use_manufactured_solns_for_advance = false
n_ion_species = 1
n_neutral_species = 0
electron_physics = "boltzmann_electron_response"
#electron_physics = "boltzmann_electron_response_with_simple_sheath"
run_name = "1D-wall_evolve_nel_r_1_z_9_vpa_8_vperp_8_krook_diss"
evolve_moments_density = false
evolve_moments_parallel_flow = false
evolve_moments_parallel_pressure = false
evolve_moments_conservation = false
force_Er_zero_at_wall = false #true
Er_constant = 0.0
epsilon_offset = 0.1
use_vpabar_in_mms_dfni = true
T_e = 1.0
T_wall = 1.0
rhostar = 1.0
Bzed = 1.0
Bmag = 1.0
initial_density1 = 0.5
initial_temperature1 = 1.0
initial_density2 = 0.5
initial_temperature2 = 1.0
z_IC_option1 = "sinusoid"
z_IC_density_amplitude1 = 0.001
z_IC_density_phase1 = 0.0
z_IC_upar_amplitude1 = 0.0
z_IC_upar_phase1 = 0.0
z_IC_temperature_amplitude1 = 0.0
z_IC_temperature_phase1 = 0.0
z_IC_option2 = "sinusoid"
z_IC_density_amplitude2 = 0.001
z_IC_density_phase2 = 0.0
z_IC_upar_amplitude2 = 0.0
z_IC_upar_phase2 = 0.0
z_IC_temperature_amplitude2 = 0.0
z_IC_temperature_phase2 = 0.0
charge_exchange_frequency = 0.0
ionization_frequency = 1.0
```

```
constant_ionization_rate = true
nuii_krook = 0.1
nuii_pitch = 0.0
nstep = 20000
dt = 0.0005
nwrite = 200
nwrite_dfns = 200
use_semi_lagrange = false
n_rk_stages = 4
split_operators = false
z_ngrid = 17
z_nelement = 9
z_nelement_local = 9
z_bc = "wall"
z_discretization = "chebyshev_pseudospectral"
r_ngrid = 1
r_nelement = 1
r_nelement_local = 1
r_bc = "periodic"
r_discretization = "chebyshev_pseudospectral"
vpa_ngrid = 17
vpa_nelement = 8
vpa_L = 6.0
vpa_bc = "zero"
vpa_discretization = "chebyshev_pseudospectral"
vperp_ngrid = 17
vperp_nelement = 8
vperp_L = 3.0
vperp_bc = "periodic"
#vperp_discretization = "finite_difference"
vperp_discretization = "chebyshev_pseudospectral"

vz_ngrid = 17
vz_nelement = 4
vz_L = 12.0
vz_bc = "periodic"
vz_discretization = "chebyshev_pseudospectral"

vr_ngrid = 17
vr_nelement = 4
vr_L = 12.0
vr_bc = "periodic"
```

```
vr_discretization = "chebyshev_pseudospectral"

vzeta_ngrid = 17
vzeta_nelement = 4
vzeta_L = 12.0
vzeta_bc = "periodic"
vzeta_discretization = "chebyshev_pseudospectral"

[numerical_dissipation]
vpa_dissipation_coefficient = 0.01
#z_dissipation_coefficient = 0.1
r_dissipation_coefficient = 0.0
```


[1] Helander P and Sigmar D J 2002 *Collisional Transport in Magnetized Plasmas* (Cambridge, UK: Cambrige University Press)

[2] Abel I G, Plunk G G, Wang E, Barnes M, Cowley S C, Dorland W and Schekochihin A 2013 *Rep. Prog. Phys.* **76** 116201

[3] Schekochihin A, Cowley S, Dorland W, Hammett G, Howes G G, Plunk G, Quataert E and Tatsuno T 2008 *Plasma Phys. Control. Fusion* **50** 124024

[4] Barnes M, Dorland W and Tatsuno T 2010 *Physics of Plasmas* **17** 032106

[5] Abazorius M 2023 *University of Oxford* DPhil Thesis *(In Progress)*

[6] Rosenbluth M N, MacDonald W M and Judd D L 1957 *Phys. Rev.* **107** 1–6

[7] Bhatnagar P L, Gross E P and Krook M 1954 *Phys. Rev.* **94** 511–525

[8] Parra F I, Barnes M and Hardman M R 2021 *Excalibur/Neptune Report* 2047357–TN–07–01 M1.4

[9] Hazeltine R D and Meiss J D 2003 *Plasma Confinement* (New York: Dover)

[10] Boyd J P 2001 *Chebyshev and Fourier Spectral Methods* (Dover)

[11] Hirvijoki E and Adams M F 2017 *Phys. Plasmas* **24** 032121

[12] Hardman M R, Omotani J, Barnes M, Newton S L and Parra F I 2023 *Excalibur/Neptune Report 2070839-TN-04*

[13] Alouani-Bibi F, Shoucri M and Matte J P 2004 *Computer physics communications* **164** 60–66

[14] Pataki A and Greengard L 2011 *Journal of Computational Physics* **230** 7840–7852